

# High-Performance Selective CO<sub>2</sub> Capture on a Stable and Flexible Metal–Organic Framework via Discriminatory Gate-Opening Effect

Junjie Peng,<sup>1</sup> Zewei Liu,<sup>1</sup> Ying Wu, Shikai Xian,\* and Zhong Li\*Cite This: <https://doi.org/10.1021/acsami.2c04779>

Read Online

ACCESS |



Metrics &amp; More



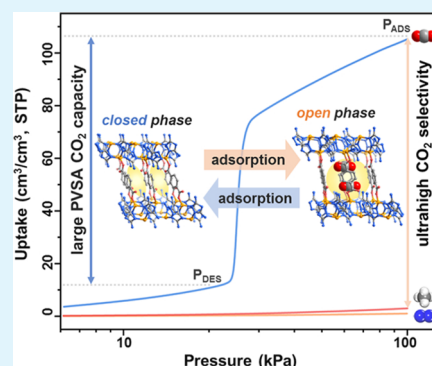
Article Recommendations



Supporting Information

**ABSTRACT:** Selective CO<sub>2</sub> capture is of great significance for environmental protection and industrial demand. Here, we report a stable and flexible metal–organic framework (MOF) with excellent water/moisture stability, namely, ZnDatzBdc, that enables high-performance selective CO<sub>2</sub> capture from N<sub>2</sub> and CH<sub>4</sub> via a discriminatory gate-opening effect. ZnDatzBdc shows reversible structural transformation between the open-phase (OP) state and the close-phase (CP) state, owing to the synergistic effect of breakage/re-formation of intraframework hydrogen bonds and the rotation of the phenyl rings. Significantly, ZnDatzBdc exhibits S-shaped isotherms toward CO<sub>2</sub>, resulting in a large CO<sub>2</sub> theoretical working capacity of 94.9 cm<sup>3</sup>/cm<sup>3</sup> under typical pressure vacuum swing adsorption (PVSA) operations, which outperforms other flexible MOFs showing the CO<sub>2</sub> selective gate-opening effect except for the moisture-sensitive ELM-11. In addition, CO<sub>2</sub> uptake of ZnDatzBdc is well maintained upon multiple water/moisture exposure, indicating its excellent stability. Moreover, ZnDatzBdc establishes remarkable CO<sub>2</sub> selectivity with ultrahigh uptake ratios of CO<sub>2</sub>/N<sub>2</sub> (107 at 273 K and 129 at 298 K) and CO<sub>2</sub>/CH<sub>4</sub> (35 at 273 K and 44 at 298 K) at 100 kPa. The in situ gas sorption PXRD experiment verifies that the gate-opening effect takes place in the atmospheric environment of CO<sub>2</sub> but not for N<sub>2</sub> or CH<sub>4</sub>. Molecular simulation suggests the selective gate-opening of CO<sub>2</sub> comes from its strong electrostatic interactions with the amino groups. Furthermore, effective breakthrough performance and easy regeneration are further confirmed. Hence, combined with excellent separation performance and remarkable stability, ZnDatzBdc can serve as a potential industrial adsorbent for selective CO<sub>2</sub> capture.

**KEYWORDS:** selective CO<sub>2</sub> capture, adsorption, metal–organic framework, flexibility, gas separation



## INTRODUCTION

The ever-increasing concentration of greenhouse gases, especially CO<sub>2</sub> with an annual emission of over 32 gigatons,<sup>1</sup> is causing severe climate issues, such as melting glaciers, rising sea level, abnormal climate, and ecosystem change.<sup>2–4</sup> A key contributor to anthropogenic CO<sub>2</sub> is the exhaust gas from fossil fuel burning mainly composed of CO<sub>2</sub> and N<sub>2</sub>. In addition, natural gas and biogas are cheap and clean energy resources, with CH<sub>4</sub> as the efficient component. However, the coexistence of a considerable amount of CO<sub>2</sub> will significantly lower the calorific value and cause corrosion to the facilities during storage and transportation. Hence, selective CO<sub>2</sub> separation from their gas mixtures is of great importance for environmental protection and industrial demand.<sup>5–8</sup>

Among current strategies for carbon capture, adsorption is recognized as a promising separation technology with plausible enhancement in energy efficiency and cost reductions.<sup>9–12</sup> The properties of the adsorbent have a direct impact on the adsorption performance, including working capacity, selectivity, kinetics, adsorption heat, and regeneration conditions.<sup>10</sup> By now, extensive studies have attempted to establish high equilibrium capacity and selectivity of CO<sub>2</sub> on various types of adsorbents with typical Langmuir-type adsorption iso-

therms, including zeolites, silicas, activated carbons, and MOFs,<sup>5,9–16</sup> whereas for a practical PVSA system, a high equilibrium capacity does not always result in a high working capacity on these adsorbents. Because the uptake increment decreases gradually with the rising temperature on typical Langmuir-type isotherms, a considerable amount of CO<sub>2</sub> uptake cannot be regenerated in the desorption process (Figure S1), which would lower the working capacity dramatically.<sup>17–20</sup> In contrast, an adsorbent with an S-shaped CO<sub>2</sub> isotherm would be more desirable.<sup>17</sup> As shown in Figure 1, the CO<sub>2</sub> uptake is small at low pressure but increases sharply when reaching the threshold pressure so that most of the adsorbed CO<sub>2</sub> molecules can be liberated in the PVSA operations, resulting in an enhanced CO<sub>2</sub> working capacity. Benefiting from the structural transformation from their CP state to OP state, some flexible metal–organic frameworks

Received: March 17, 2022

Accepted: April 18, 2022

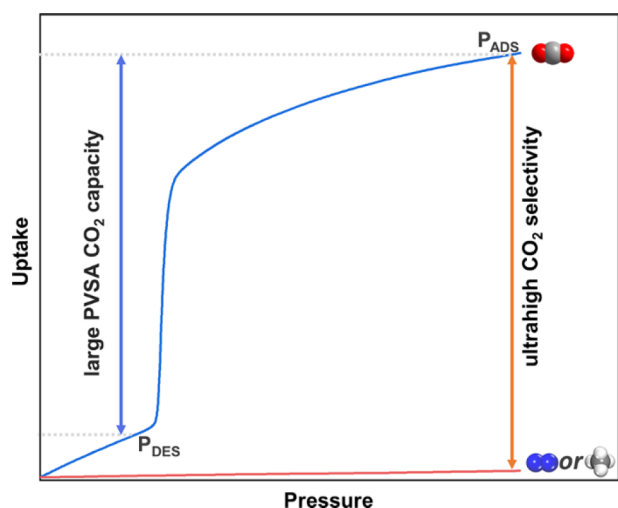


**Figure 1.** Advantages of flexible MOFs for high-performance selective carbon capture in PVSA processes.  $P_{\text{ADS}}$  and  $P_{\text{DES}}$  are the pressure of adsorption and pressure of desorption, respectively.

(MOFs) can exhibit such S-shaped  $\text{CO}_2$  isotherms.<sup>21–24</sup> In addition, since each guest molecule has its own gate-opening pressure, high selectivity of gas mixtures can be achieved by this distinction when the target molecule can open the gate and others cannot.<sup>21,22,25</sup> Hence, flexible MOFs with S-shaped isotherms might serve as potential adsorbents for carbon capture combined with good working capacity and high selectivity toward  $\text{CO}_2$ .

Besides separation performance, stability is also an important factor that determine the industrial utility of adsorbents.<sup>26,27</sup> Though some flexible MOFs demonstrate

potential for selective  $\text{CO}_2$  capture, their industrial employment still remains a challenge. On one hand, the actual feed gases usually contain a trace amount of water, so water/moisture robustness is requisite for industrial adsorbents.<sup>28,29</sup> However, some MOFs with excellent  $\text{CO}_2$  capture performance exhibit poor chemical stability or remain elusive on their chemical stability.<sup>30–34</sup> For example, ELM-11 holds excellent  $\text{CO}_2$  volumetric uptake and high theoretical  $\text{CO}_2$  working capacity under PVSA operations, but its structure is easily damaged and the  $\text{CO}_2$  capacity is lost dramatically after a few cycles with contact of moist air.<sup>17,31,35,36</sup> On the other hand, some stable MOFs such as ZIF-7<sup>37,38</sup> only show moderate volumetric uptake and working capacity toward  $\text{CO}_2$ . Hence, there is still a great demand to rationally develop more innovative flexible materials with both excellent separation performance and high water/moisture stability.

Herein, we synthesized a new flexible MOF, termed ZnDatzBdc (Datz = 3,5-diamine-1,2,4-triazolate, Bdc = 1,4-benzenedicarboxylate), that enables high-performance selective  $\text{CO}_2$  capture. The reversible structural transformation between its OP state and the CP state was confirmed by X-ray diffraction studies. Importantly, ZnDatzBdc shows S-shaped isotherms of  $\text{CO}_2$ , resulting in an appreciable  $\text{CO}_2$  working capacity of  $94.9 \text{ cm}^3/\text{cm}^3$  under typical PVSA operations at 273 K, which outperforms most reported flexible MOFs except for the moisture-sensitive ELM-11. Moreover, the uptake of  $\text{N}_2$  or  $\text{CH}_4$  was negligible at near atmospheric conditions, giving rise to ultrahigh uptake ratios toward  $\text{CO}_2/\text{N}_2$  and  $\text{CO}_2/\text{CH}_4$ . The PXRD patterns and  $\text{CO}_2$  adsorption capacity were well maintained after multiple water/moisture treatments, verifying its excellent water/moisture stability. The selective gate-opening mechanism toward  $\text{CO}_2$  adsorption was illustrated by in situ gas sorption PXRD measurement and molecular

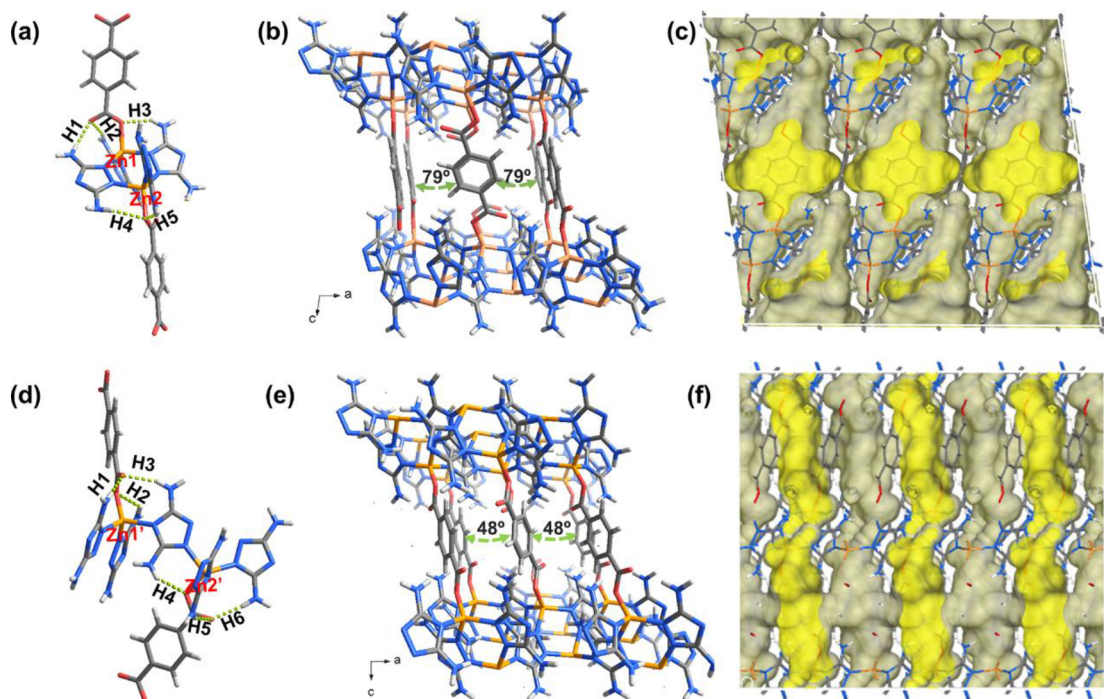


**Figure 2.** Coordination environment (a), crystal structure on the  $b$ -axis (b), and the Connolly surface on the  $b$ -axis (c) of ZnDatzBdc\_OP; coordination environment (d), crystal structure on the  $b$ -axis (e), and the Connolly surface on the  $b$ -axis (f) of ZnDatzBdc\_CP. Orange, blue, red, gray, and light gray dots represent Zn, N, O, C, and H atoms, respectively. The green dotted linear lines represent the hydrogen bonds. The Connolly surface was calculated using a probe with a radius of 1 Å.

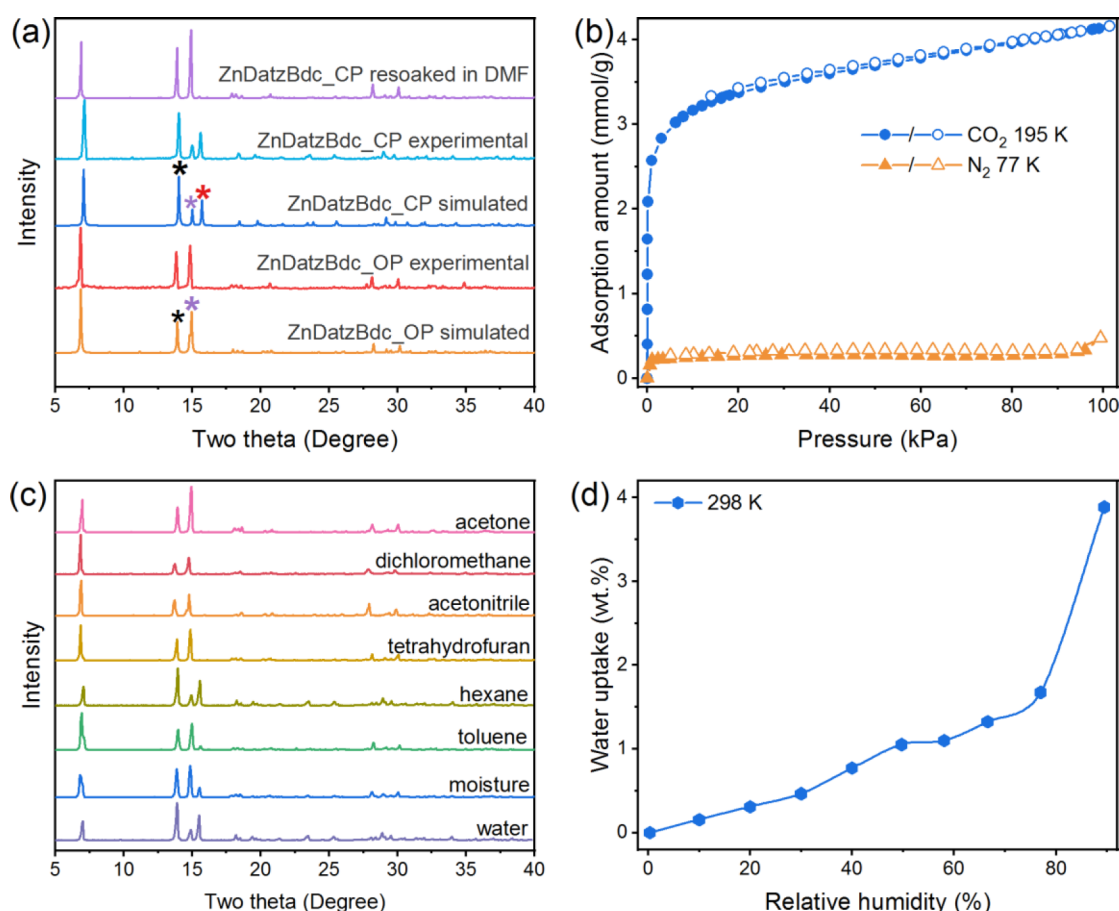


**Figure 3.** (a) PXRD patterns of ZnDatzBdc\_OP, ZnDatzBdc\_CP, and ZnDatzBdc\_CP res soaked in DMF, compared to the simulated ones derived from the SCXRD data; (b) sorption isotherms of CO<sub>2</sub> at 195 K and N<sub>2</sub> at 77 K (solid and open dots represent adsorption and desorption, respectively); (c) PXRD patterns of ZnDatzBdc after treatment with water, moisture, or common organic solvents for 3 days; (d) water vapor adsorption isotherm of ZnDatzBdc at 298 K.

simulation on the preferential adsorption sites. Finally, the cyclable breakthrough experiment under gentle regeneration conditions indicates the effective real-world separation toward CO<sub>2</sub>/CH<sub>4</sub> and CO<sub>2</sub>/N<sub>2</sub> mixtures.

## EXPERIMENTAL SECTION

**Synthesis of ZnDatzBdc-DMF.** 1,4-Benzenedicarboxylic acid (H<sub>2</sub>Bdc, 167 mg, 1 mmol) and 3,5-diamino-1H-1,2,4-triazole (HDatz, 99 mg, 1 mmol) were transferred to a 20 mL autoclave, and subsequently a binary solution was added, combined of 2 mL of *N,N'*-dimethylformamide (DMF) and 8 mL of H<sub>2</sub>O dissolving Zn(NO<sub>3</sub>)<sub>2</sub>·6H<sub>2</sub>O (297 mg, 1 mmol). The suspension was dispersed by sonication, and then the autoclave was sealed and placed in a preheated oven at 423 K for 60 h. Afterward, the autoclave was cooled to ambient temperature at a rate of 10 K/h. The resultant plate crystals were collected by filtration, washed with DMF, and then dried in air. Elemental analysis calculated for C<sub>54</sub>H<sub>62</sub>N<sub>42</sub>O<sub>18</sub>Zn<sub>8</sub> (Zn<sub>8</sub>(Datz)<sub>8</sub>(Bdc)<sub>4</sub>·2DMF): C, 30.73; H, 2.96; N, 27.88. Found: C, 30.28; H, 2.73; N, 27.63. CCDC number: 2118619.

**Synthesis of ZnDatzBdc\_CP.** ZnDatzBdc-DMF was soaked in DMF for 2 days to remove the residual reactants, followed by extraction with methanol (MeOH) for 3 days to remove the DMF molecules. The solvent was exchanged twice per day. After solvent extraction, the crystals were activated carefully under a high vacuum to afford ZnDatzBdc\_CP suitable for SCXRD analysis. Elemental analysis calculated for C<sub>24</sub>H<sub>24</sub>N<sub>20</sub>O<sub>8</sub>Zn<sub>4</sub> (Zn<sub>4</sub>(Datz)<sub>4</sub>(Bdc)<sub>2</sub>): C, 29.35; H, 2.46; N, 28.52. Found: C, 29.15; H, 2.31; N, 28.36. CCDC number: 2118618.

## RESULTS AND DISCUSSION

**Crystal Structure and Pore Properties.** Single-crystal XRD measurement reveals that ZnDatzBdc-DMF crystallizes in the monoclinic system and *P2<sub>1</sub>/c* space group (*a* = 9.9598 Å, *b* = 8.3253 Å, *c* = 25.9861 Å,  $\beta$  = 98.159°), with a unit cell volume of 2132.9 Å<sup>3</sup> (Table S1). In ZnDatzBdc-DMF, Zn<sup>2+</sup> ions adopt a tetrahedral coordination mode (Figure 2a), while Bdc<sup>2-</sup> and Datz<sup>-</sup> ligands coordinate with two and three Zn<sup>2+</sup> ions, respectively, resulting in a pillared-layered structure (Figure 2b). In addition, two crystallographically unique positions of the phenyl rings exist in the framework, with a dihedral angle of 79°. Since the DMF molecule is incorporated in the structure, ZnDatzBdc-DMF is in the OP state, and hence it is also denoted as ZnDatzBdc\_OP. Intriguingly, according to the definition of hydrogen bonds, multiple labile intraframework hydrogen bonds are formed between the amine groups and the oxygen atoms,<sup>39,40</sup> and the details about these hydrogen bonds are listed in Table S2. In addition, a hydrogen bond is formed between the oxygen atom from the DMF molecule and the -NH<sub>2</sub> group (Figure S2). After solvent exchange and removal, ZnDatzBdc\_OP transforms into ZnDatzBdc\_CP, suggesting apparent flexibility of this compound (Figure 2d,e). ZnDatzBdc\_CP has the same connectivity and crystal system but belongs to a more symmetric *I2/c* space group (*a* = 9.6070 Å, *b* = 8.3705 Å, *c* = 24.955 Å,  $\beta$  = 90.097°) with a contracted unit cell volume of



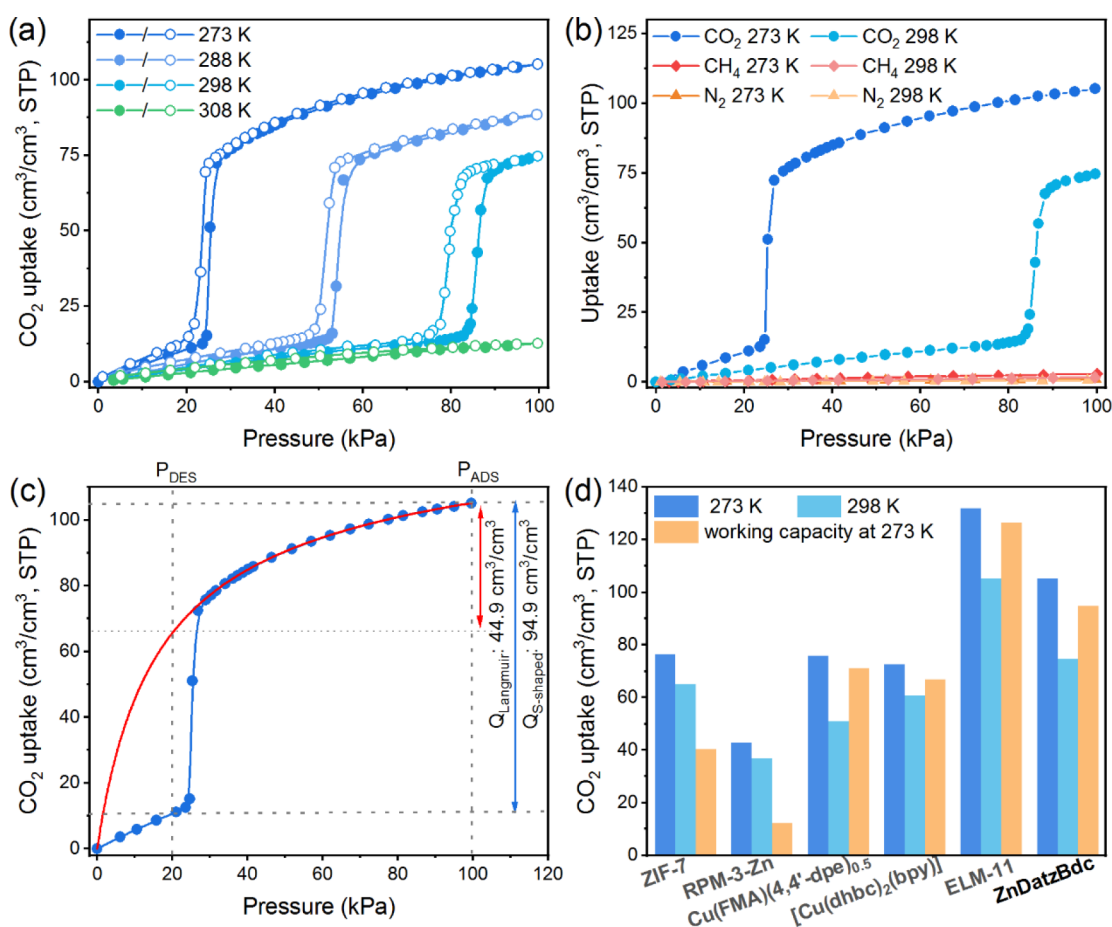


**Figure 4.** (a) Single-component CO<sub>2</sub> isotherms on ZnDatzBdc up to 100 kPa and varied temperatures (solid and open dots represent adsorption and desorption, respectively); (b) adsorption isotherms of CO<sub>2</sub>, N<sub>2</sub>, and CH<sub>4</sub> up to 100 kPa at 273 and 298 K; (c) CO<sub>2</sub> working capacities for the step-shaped isotherm of ZnDatzBdc and the simulated Langmuir isotherm in the open phase, for a cycle of adsorption at 100 kPa and desorption at 20 kPa (273 K); (d) comparison of CO<sub>2</sub> uptakes and working capacities of ZnDatzBdc and other flexible MOFs with S-shaped CO<sub>2</sub> isotherms.

2006.8 Å<sup>3</sup>. For ZnDatzBdc\_CP, the angle between the phenyl rings of the two different positions is reduced to 48° and more intraframework hydrogen bonds are formed compared with ZnDatzBdc\_OP. Hence, we speculate that the dynamic transformation of this MOF structure originates from the easy breakage/re-formation of its high-density labile hydrogen bonds and the associated rotation of phenyl rings.<sup>41,42</sup> Vice versa, for MOFs with fewer hydrogen bonds, it is difficult to achieve apparent flexibility due to a less stable potential CP state sustained by fewer hydrogen bonds. Taking Zn(atz)-(bdc)<sub>0.5</sub> as an example, an isorecticular structure of ZnDatzBdc with fewer intramolecular hydrogen bonds (Figure S3), it does not exhibit apparent phase-change behavior upon activation, as evidenced by PXRD and CO<sub>2</sub> isotherms, which suggests the number of intramolecular hydrogen bonds plays an important role in flexibility.<sup>43</sup> To evaluate the pore system, the Connolly surface was calculated by using Material Studio 7.0 (Figures 2c,f, S4, and S5).<sup>44</sup> ZnDatzBdc\_OP holds zigzag cavities in a spindle shape with a cross-section size of 4.9 × 6.7 Å<sup>2</sup> (the van der Waals radius is considered). When ZnDatzBdc transforms to ZnDatzBdc\_CP, the large cavity of ZnDatzBdc\_OP is split into two smaller cavities with a narrow cross-section size of 2.4 × 4.9 Å<sup>2</sup>, which might prohibit the accessibility of many adsorbates.

**Characterizations and Stability.** The phase purity was confirmed by comparing the experimental and calculated element contents and PXRD patterns (Figure 3a). For ZnDatzBdc\_OP and ZnDatzBdc\_CP, their PXRD patterns looked overall similar, but multiple differences were observed on both the positions and intensities of the diffraction peaks, such as apparent increase of the peak of 13.9°, reduction of the peak at 15.0°, and appearance of a new peak at 15.8°. Hence, the PXRD pattern can act as a straightforward feature to distinguish the OP state and CP state of this flexible MOF. When ZnDatzBdc\_CP was res soaked in DMF, the PXRD pattern suggested the CP state shifted into the OP state, verifying the reversible flexibility of this structure. Due to failure of the gate-opening by N<sub>2</sub>, ZnDatzBdc showed a low N<sub>2</sub> uptake of 0.48 mmol/g at 77 K (Figure 3b). Thus, the porosity was evaluated by CO<sub>2</sub> adsorption at 195 K (4.13 mmol/g at 100 kPa), giving a BET surface area of 303 m<sup>2</sup>/g and a pore volume of 0.11 cm<sup>3</sup>/g. Thermogravimetric analysis (Figure S6) and in situ variable temperature PXRD patterns (Figure S7) indicate that this MOF possesses excellent thermal stability with a high decomposition temperature of about 710 K. Moreover, ZnDatzBdc can survive in water, moisture, and common organic solvents for 3 days, as suggested by the PXRD patterns (Figure 3c). It is noticed that the water uptake was only about 4 wt % at high relative humidity of 90% and

298 K (Figure 3d). Such small water uptake might come from the high-density hydrophobic phenyl rings and the intraframework hydrogen bonds that weaken the interaction toward water molecules.<sup>40,45</sup>

**Isotherms of CO<sub>2</sub>, N<sub>2</sub>, and CH<sub>4</sub>.** Encouraged by the apparent flexibility of ZnDatzBdc, we measured the single-component isotherms of CO<sub>2</sub>, N<sub>2</sub>, and CH<sub>4</sub> to investigate its potential for selective CO<sub>2</sub> capture. As shown in Figure 4a, S-shaped CO<sub>2</sub> sorption isotherms were observed at temperatures of 273, 288, and 298 K, with corresponding threshold pressures of 25, 53, and 83 kPa. As the gate-opening pressure increased with the rising temperature, a linear CO<sub>2</sub> isotherm was discovered instead of an S-shaped isotherm at 308 K due to a gate-opening pressure over atmospheric conditions. In addition, a high goodness-of-fit can be obtained by plotting the threshold pressures versus the inverse of temperature (Figure S8), which can be used to predict the threshold pressure at desired operating temperatures. It is also noticed that the hysteresis was small, indicating a readily structural transformation process.<sup>21</sup> While ZnDatzBdc took up only about 13.8 cm<sup>3</sup>/cm<sup>3</sup> CO<sub>2</sub> (0.38 mmol/g) before it opened the gate, the CO<sub>2</sub> uptake increased sharply at the gate-opening pressure and reached 105.2 cm<sup>3</sup>/cm<sup>3</sup> (2.89 mmol/g) and 74.7 cm<sup>3</sup>/cm<sup>3</sup> (2.05 mmol/g) at atmospheric pressure for 273 and 298 K, respectively. Moreover, the CO<sub>2</sub> adsorption isotherms were fully reproducible over five adsorption–desorption cycles at 273 K (Figure S9).

Due to the narrow channels at the CP state and failure to open the pores, ZnDatzBdc showed negligible uptakes for N<sub>2</sub> (0.99 cm<sup>3</sup>/cm<sup>3</sup> at 273 K, 0.58 cm<sup>3</sup>/cm<sup>3</sup> at 298 K) and CH<sub>4</sub> (2.96 cm<sup>3</sup>/cm<sup>3</sup> at 273 K, 1.73 cm<sup>3</sup>/cm<sup>3</sup> at 298 K) at atmospheric pressure. The resultant uptake ratios at 100 kPa of CO<sub>2</sub>/N<sub>2</sub> and CO<sub>2</sub>/CH<sub>4</sub> reach as high as 129 and 44 at 298 K as well as 107 and 35 at 273 K separately, which are comparatively high when compared to those of other flexible MOFs exhibiting S-shaped isotherms toward CO<sub>2</sub> (Table S3).<sup>30–33,37,38</sup>

For a practical PVSA unit, an important parameter to determine the feasibility of an adsorbent is the usable capacity of target molecules.<sup>26,27</sup> The theoretical working capacities of CO<sub>2</sub> at 273 K were calculated based on the adsorption isotherm, assuming the adsorption pressure at 100 kPa and the desorption pressure at 20 kPa according to a typical PVSA operating condition.<sup>46</sup> Figure 4c shows 94.9 cm<sup>3</sup>/cm<sup>3</sup> CO<sub>2</sub> can be recycled on ZnDatzBdc under this operation condition, about 90% of the equilibrium uptake at 100 kPa. This is because most of the adsorbed CO<sub>2</sub> molecules can be liberated in a desorption pressure lower than the gate-opening pressure (25 kPa). For comparison, a simulated CO<sub>2</sub> Langmuir isotherm was obtained by using the experimental adsorption data in the OP state. In contrast, only 44.9 cm<sup>3</sup>/cm<sup>3</sup> CO<sub>2</sub> is reproducible for the simulated Langmuir equation under the same operation condition, accounting for 43% of the CO<sub>2</sub> equilibrium uptake. Hence, higher usable capacities can be achieved on flexible MOFs with S-shaped isotherms than adsorbents with typical Langmuir isotherms. In addition, the equilibrium capacity and working capacity was also compared with that of other flexible MOFs exhibiting selective S-shaped isotherms toward CO<sub>2</sub> (Figure 4d and Table S4).<sup>30–33,38</sup> At atmospheric pressure, ZnDatzBdc shows higher CO<sub>2</sub> volumetric uptake than other reported flexible MOFs except for the benchmark material ELM-11 at both 273 and 298 K. Similarly, the CO<sub>2</sub> theoretical capacity of ZnDatzBdc is higher than that

of ZIF-7 (40.2 cm<sup>3</sup>/cm<sup>3</sup>), Cu(FMA)(4,4'-dpe)<sub>0.5</sub> (71.2 cm<sup>3</sup>/cm<sup>3</sup>), [Cu(dhbc)<sub>2</sub>(bpy)] (66.8 cm<sup>3</sup>/cm<sup>3</sup>), and RPM-3-Zn (12.2 cm<sup>3</sup>/cm<sup>3</sup>) and only second to that of ELM-11 (126.5 cm<sup>3</sup>/cm<sup>3</sup>). However, ELM-11 shows irreversible structural decomposition and considerable capacity loss upon moisture contact.<sup>35</sup> By contrast, the CO<sub>2</sub> capacity of ZnDatzBdc exhibited no apparent loss after four times of cyclic exposure upon water and moisture (Figures S10 and S11), confirming its excellent stability. Hence, considering the balance between CO<sub>2</sub> working capacity and stability, ZnDatzBdc is more promising than the benchmark ELM-11 in the long term industrial CO<sub>2</sub> capture.

**Insight into Selective Gate-Opening of CO<sub>2</sub>.** To access the structural transition of ZnDatzBdc\_CP upon exposure to different guest molecules, in situ gas sorption PXRD measurements were performed at 298 K (Figure 5). Under

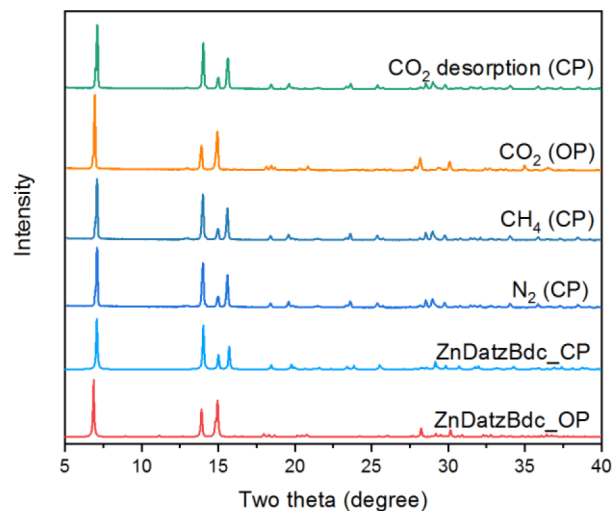


**Figure 5.** PXRD patterns of ZnDatzBdc under different gas atmosphere.

atmospheric N<sub>2</sub> or CH<sub>4</sub>, no PXRD changes took place, suggesting the structure retained its CP state. By contrast, when atmospheric CO<sub>2</sub> was injected, PXRD patterns showed distinct changes and were almost identical to that of ZnDatzBdc\_OP, indicative of transformation from the CP state to the OP state. After CO<sub>2</sub> adsorption, flowing He was utilized to desorb the loading CO<sub>2</sub> molecules at 298 K. As a result, complete reversion back to the CP state took place, suggesting that the adsorbed CO<sub>2</sub> was readily removed in a mild desorption condition.

To our knowledge, it is generally accepted that the stronger the interaction between the guest molecules and the adsorbent is, the lower the gate-opening pressure.<sup>22</sup> Hence, CO<sub>2</sub> with higher polarizability ( $29.11 \times 10^{-25}$  cm<sup>3</sup>) than CH<sub>4</sub> ( $25.93 \times 10^{-25}$  cm<sup>3</sup>) and N<sub>2</sub> ( $17.403 \times 10^{-25}$  cm<sup>3</sup>) would form stronger interactions with the structure and exhibit lower gate-opening pressure.<sup>21</sup> In accordance with the assumption, the high-pressure adsorption isotherms (Figure S12) showed the gate-opening pressure order of CO<sub>2</sub> < CH<sub>4</sub> < N<sub>2</sub>. To elucidate the detailed interactions between the guest molecules and the framework, the preferential gas adsorption sites on ZnDatzBdc\_OP were calculated, as shown in Figure 6. Notably, CO<sub>2</sub> forms two N–H⋯O electrostatic interactions with the amino groups. In addition, weaker dispersion interactions were observed between CO<sub>2</sub> and three phenyl/triazolate rings. For

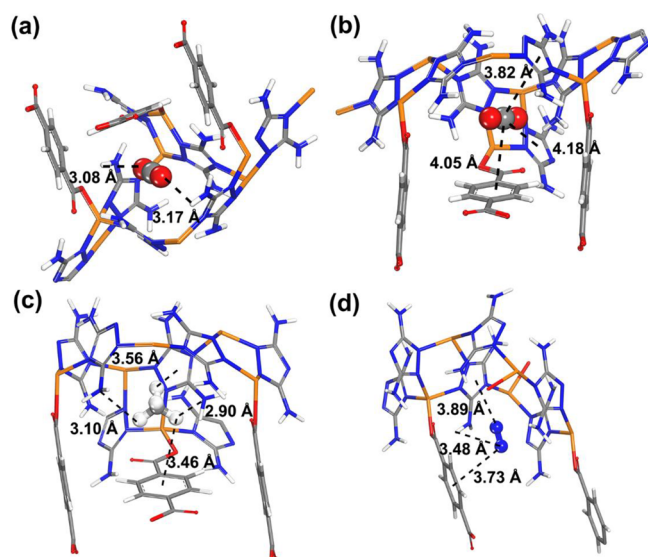


**Figure 6.** Simulated preferential adsorption sites of guest molecules in ZnDatzBdc\_OP: (a) CO<sub>2</sub> interacts with H atoms from amino group; (b) CO<sub>2</sub> interacts with the adjacent triazolate/phenyl rings; (c) CH<sub>4</sub> interacts with N atoms from amino group and the adjacent triazolate/phenyl rings; (d) N<sub>2</sub> interacts with H atoms from amino groups and the adjacent triazolate/phenyl rings. Orange, blue, red, gray, and light gray dots represent Zn, N, O, C, and H atoms, respectively.

CH<sub>4</sub>, it prefers to be fixed by two amino groups and two phenyl/triazolate rings through dispersion interactions. However, considering the less polarized C–H bonds of CH<sub>4</sub>, their dispersion interactions are much weaker compared to electrostatic interactions and dispersion interactions between CO<sub>2</sub> and ZnDatzBdc, despite the shorter distance of the contact atoms. For N<sub>2</sub>, only weak dispersion interactions were formed with one amine group and two triazolate/phenyl rings. These simulation results revealed that the preferential interaction between the gas molecules and the frameworks follows the order of CO<sub>2</sub> > CH<sub>4</sub> > N<sub>2</sub>. Hence, it is reasonable to assume that the selective gate-opening of CO<sub>2</sub> on ZnDatzBdc originates from the stronger interactions of CO<sub>2</sub> than that of N<sub>2</sub> and CH<sub>4</sub>.

**Intrinsic Thermal Management.** Besides equilibrium cyclable capacity and selectivity, one important but often neglected concern in industrial PVSA operations is thermal management during the adsorption process. If these heat effects are substantial, a large temperature swing occurs during the adsorption operation and thus the usable capacity is lessened significantly.<sup>17,20</sup> For flexible MOFs, the opening of the framework is an endothermic process, and thus the adsorption heat and even the energy input in desorption can be partially suppressed. To confirm the energy difference of the OP and CP states, the single atomic energies of optimized MOFs were calculated and an energy gap of +38.9 kJ/mol (kilojoule per mol unit cell) was observed between the OP and CP states. In addition, the adsorption enthalpy of CO<sub>2</sub> was estimated by calculating the isosteric heat (Figure 7) with the Clausius–Clapeyron equation from the CO<sub>2</sub> adsorption isotherms (Figures S13–S15).<sup>47,48</sup> Before the gate-opening pressure (uptake of <0.4 mmol/g), the isosteric heat of CO<sub>2</sub> was about 26–29 kJ/mol. When the gate-opening occurred, the isosteric heat of CO<sub>2</sub> was increased to 32.5–34.5 kJ/mol. Such an increment might come from the strong electrostatic interactions between CO<sub>2</sub> and the free –NH<sub>2</sub> group after pore

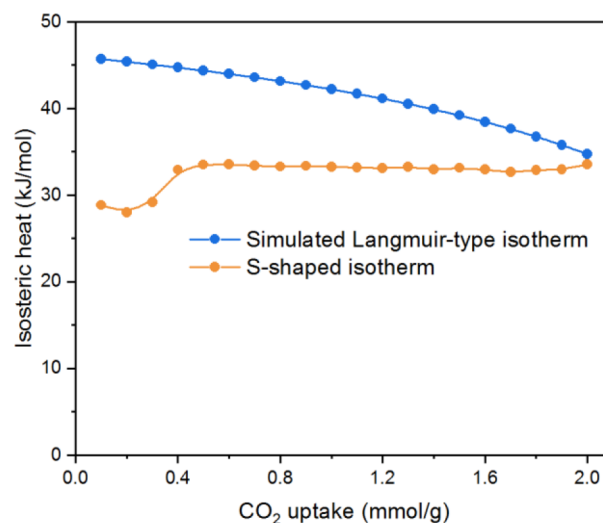


**Figure 7.** Isosteric heat of CO<sub>2</sub> on ZnDatzBdc featuring S-shaped isotherms and the simulated adsorbent with Langmuir-type isotherms.

opening. For comparison, by applying a previously reported method,<sup>20,49</sup> we simulated the Langmuir-type CO<sub>2</sub> isotherms for ZnDatzBdc by using the adsorption data in the OP state (Figures S16–S18), and the resultant isosteric heat was found to be 45.7–34.7 kJ/mol (Figure 7). Thus, the average heat released upon CO<sub>2</sub> adsorption can be offset by about 22% due to the gate opening effect, indicating effective intrinsic thermal management of ZnDatzBdc during the CO<sub>2</sub> adsorption process.

**Breakthrough Separation Performance.** In order to evaluate the practical feasibility of ZnDatzBdc for carbon capture, the real-time breakthrough experiments were performed to mimic the dynamic separation performance toward equimolar CO<sub>2</sub>/N<sub>2</sub> and CO<sub>2</sub>/CH<sub>4</sub> binary mixtures at 273 K, as shown in Figure 8. CH<sub>4</sub> and N<sub>2</sub> broke through shortly after introduction of the gas mixtures, indicative of their negligible uptake on ZnDatzBdc. Nevertheless, CO<sub>2</sub> breakthrough occurred at 10.1 and 9.1 min for CO<sub>2</sub>/N<sub>2</sub> and CO<sub>2</sub>/CH<sub>4</sub> mixtures, respectively. When adsorption reached equilibrium for the two mixtures, the corresponding CO<sub>2</sub> working capacities were 82.1 cm<sup>3</sup>/cm<sup>3</sup> (2.25 mmol/g) and 70.9 cm<sup>3</sup>/cm<sup>3</sup> (1.95 mmol/g) for CO<sub>2</sub>/N<sub>2</sub> and CO<sub>2</sub>/CH<sub>4</sub> mixtures. Subsequently, to mimic the gentle regeneration of the PVSA process, the adsorption column was purged with flowing He for 30 min at 273 K (the same temperature in adsorption) to liberate the adsorbed CO<sub>2</sub> molecules. It is noted that volume ratios of the desorbed CO<sub>2</sub>/N<sub>2</sub> and CO<sub>2</sub>/CH<sub>4</sub> mixture were 76 and 11 (Figures S20 and S21), respectively, indicating high dynamic selectivity was achieved in gas mixtures. Though the dynamic selectivities were lower than those calculated from the equilibrium uptakes, it is reasonable because a small amount of N<sub>2</sub> and CH<sub>4</sub> might also enter the pores when CO<sub>2</sub> opens the gate. In addition, the CO<sub>2</sub> capacity was well-maintained for five cycles under this regeneration conditions (Figures S22–S25), suggesting that low energy input is required for regeneration. Furthermore, considering the low cost of the starting material, we performed scale-up synthesis of about 11 g of sample. The breakthrough separation performance is consistent with that of the samples prepared in milligram scales (Figures S26 and S27), which is vital for potential industrial applications.



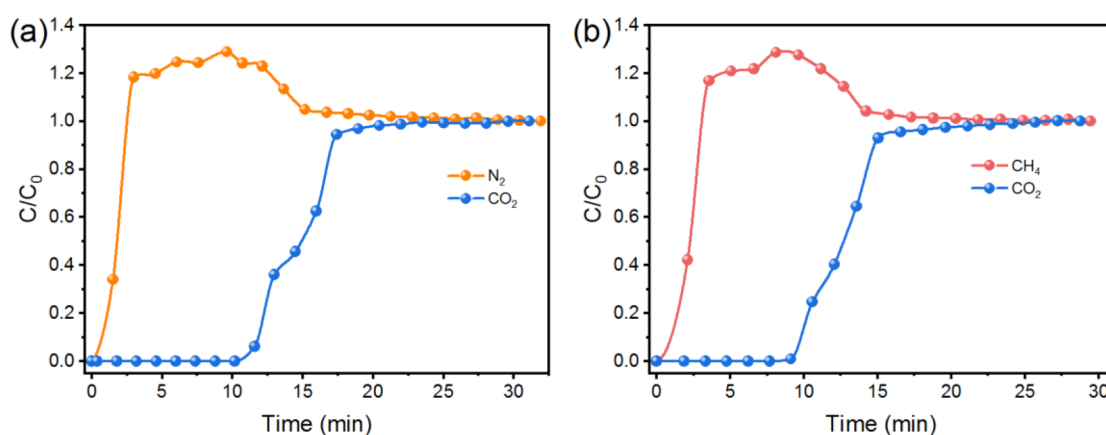


**Figure 8.** Breakthrough curves of equimolar  $\text{CO}_2/\text{N}_2$  (a) and  $\text{CO}_2/\text{CH}_4$  (b) mixtures on ZnDatzBdc at 273 K.

## CONCLUSIONS

In summary, we report a flexible MOF, namely, ZnDatzBdc, that shows high-performance selective  $\text{CO}_2$  capture via discriminatory gate-opening effect. Intriguingly, ZnDatzBdc enables reversible structural transformations between the OP state and CP state. Benefiting from its flexibility, ZnDatzBdc exhibits S-shaped isotherms for  $\text{CO}_2$  but not for  $\text{N}_2$  or  $\text{CH}_4$  at atmospheric pressure, resulting in an appreciable theoretical working capacity of  $94.9 \text{ cm}^3/\text{cm}^3$  under a typical PVSA operation and ultrahigh uptake ratios of  $\text{CO}_2/\text{N}_2$  and  $\text{CO}_2/\text{CH}_4$ . Moreover, excellent stability is verified by the well-maintained PXRD patterns and  $\text{CO}_2$  uptake upon multiple exposure upon water/moisture. In situ gas sorption PXRD experiment verifies the selective gate-opening toward  $\text{CO}_2$ , and molecular simulation reveals that the selective gate-opening toward  $\text{CO}_2$  originates from the stronger interactions of  $\text{CO}_2$ . In addition, the intrinsic thermal management is confirmed by the energy difference between the OP state and the CP state as well as moderate adsorption heat. Furthermore, cyclable breakthrough experiments under gentle regeneration conditions demonstrate its excellent performance for dynamic separation of  $\text{CO}_2/\text{N}_2$  and  $\text{CO}_2/\text{CH}_4$  mixtures, indicating its practical feasibility for selective  $\text{CO}_2$  capture. Hence, with the balance of excellent separation performance and high water/moisture stability, ZnDatzBdc can serve as a potential industrial adsorbent for  $\text{CO}_2$  capture.

## ASSOCIATED CONTENT

### Supporting Information

The Supporting Information is available free of charge at <https://pubs.acs.org/doi/10.1021/acsami.2c04779>.

Materials, scale-up synthesis, experimental and simulation methods,  $\text{CO}_2$  working capacity on adsorbents exhibiting Langmuir isotherms, supplement of crystal structures and pore properties, TG/DTG curves, variable temperature PXRD patterns, fitting of  $P_{\text{GO}}$  versus  $1/T$ , cyclic  $\text{CO}_2$  adsorption isotherms under different conditions, comparison of the selective  $\text{CO}_2$  capture performance with other flexible MOFs, fitting of the  $\text{CO}_2$  isotherms with S-shaped isotherms and simulated Langmuir isotherms, breakthrough setup, cyclic breakthrough experiments, and breakthrough performance for scale-up samples (PDF)

Crystallographic information file (CIF)

Crystallographic information file (CIF)

## AUTHOR INFORMATION

### Corresponding Authors

**Shikai Xian** – Hoffmann Institute of Advanced Materials, Shenzhen Polytechnic, Shenzhen 518055, P. R. China; Email: [xianshikai@foxmail.com](mailto:xianshikai@foxmail.com)

**Zhong Li** – School of Chemistry and Chemical Engineering, South China University of Technology, Guangzhou 510640, P. R. China; The Key Laboratory of Enhanced Heat Transfer and Energy Conversion Ministry of Education, South China University of Technology, Guangzhou 510640, P. R. China; [orcid.org/0000-0002-2796-9300](https://orcid.org/0000-0002-2796-9300); Email: [cezhli@scut.edu.cn](mailto:cezhli@scut.edu.cn)

### Authors

**Junjie Peng** – School of Chemistry and Chemical Engineering, South China University of Technology, Guangzhou 510640, P. R. China

**Zewei Liu** – School of Chemistry and Chemical Engineering, South China University of Technology, Guangzhou 510640, P. R. China; [orcid.org/0000-0001-9770-4781](https://orcid.org/0000-0001-9770-4781)

**Ying Wu** – School of Chemistry and Chemical Engineering, South China University of Technology, Guangzhou 510640, P. R. China; [orcid.org/0000-0001-5168-1051](https://orcid.org/0000-0001-5168-1051)

Complete contact information is available at: <https://pubs.acs.org/doi/10.1021/acsami.2c04779>

### Author Contributions

<sup>†</sup>J.P. and Z.L. contributed equally. The manuscript was written through contributions of all authors. All authors have given approval to the final version of the manuscript.

### Notes

The authors declare no competing financial interest.

## ACKNOWLEDGMENTS

We gratefully acknowledge financial support from National Natural Science Foundation of China (Grant 21908069 (to J.P.) and Grant 21978099 (to Z.L. and Y.W.) and China Postdoctoral Science Foundation (Grant 2020M672636 (to J.P.)).

## REFERENCES

- (1) Bourzac, K. We Have the Technology. *Nature* **2017**, *550* (7675), S66–S69.

- (2) Hurd, C. L.; Lenton, A.; Tilbrook, B.; Boyd, P. W. Current Understanding and Challenges for Oceans in a Higher-CO<sub>2</sub> World. *Nat. Clim. Change* **2018**, *8* (8), 686–694.
- (3) Seneviratne, S. I.; Rogelj, J.; Séférian, R.; Wartenburger, R.; Allen, M. R.; Cain, M.; Millar, R. J.; Ebi, K. L.; Ellis, N.; Hoegh-Guldberg, O.; et al. The Many Possible Climates from the Paris Agreement's Aim of 1.5 °C Warming. *Nature* **2018**, *558* (7708), 41–49.
- (4) Schuur, E. A.; McGuire, A. D.; Schädel, C.; Grosse, G.; Harden, J.; Hayes, D. J.; Hugelius, G.; Koven, C. D.; Kuhry, P.; Lawrence, D. M.; et al. Climate Change and the Permafrost Carbon Feedback. *Nature* **2015**, *520* (7546), 171–179.
- (5) Mukherjee, S.; Chen, S.; Bezrukov, A. A.; Mostrom, M.; Tersikh, V. V.; Franz, D.; Wang, S.-Q.; Kumar, A.; Chen, M.; Space, B.; Huang, Y.; Zaworotko, M. J. Ultramicropore Engineering by Dehydration to Enable Molecular Sieving of H<sub>2</sub> by Calcium Trimesate. *Angew. Chem., Int. Ed.* **2020**, *132* (37), 16322–16328.
- (6) Mao, V. Y.; Milner, P. J.; Lee, J.-H.; Forse, A. C.; Kim, E. J.; Siegelman, R. L.; McGuirk, C. M.; Zasada, L. B.; Neaton, J. B.; Reimer, J. A.; Long, J. R. Cooperative Carbon Dioxide Adsorption in Alcoholamine- and Alkoxyalkylamine-Functionalized Metal-Organic Frameworks. *Angew. Chem., Int. Ed.* **2020**, *59* (44), 19468–19477.
- (7) Ying, Y.; Zhang, Z.; Peh, S. B.; Karmakar, A.; Cheng, Y.; Zhang, J.; Xi, L.; Boothroyd, C.; Lam, Y. M.; Zhong, C.; Zhao, D. Pressure-Responsive Two-Dimensional Metal-Organic Framework Composite Membranes for CO<sub>2</sub> Separation. *Angew. Chem., Int. Ed.* **2021**, *133* (20), 11419–11426.
- (8) Sholl, D. S.; Lively, R. P. Seven Chemical Separations to Change the World. *Nature* **2016**, *532* (7600), 435–437.
- (9) Adil, K.; Belmabkhout, Y.; Pillai, R. S.; Cadiau, A.; Bhatt, P. M.; Assen, A. H.; Maurin, G.; Eddaoudi, M. Gas/Vapour Separation Using Ultra-Microporous Metal-Organic Frameworks: Insights into the Structure/Separation Relationship. *Chem. Soc. Rev.* **2017**, *46* (11), 3402–3430.
- (10) Oschatz, M.; Antonietti, M. A Search for Selectivity to Enable CO<sub>2</sub> Capture with Porous Adsorbents. *Energy Environ. Sci.* **2018**, *11* (1), 57–70.
- (11) Gao, W.; Liang, S.; Wang, R.; Jiang, Q.; Zhang, Y.; Zheng, Q.; Xie, B.; Toe, C. Y.; Zhu, X.; Wang, J.; et al. Industrial Carbon Dioxide Capture and Utilization: State of the Art and Future Challenges. *Chem. Soc. Rev.* **2020**, *49*, 8584–8686.
- (12) Singh, G.; Lee, J.; Karakoti, A.; Bahadur, R.; Yi, J.; Zhao, D.; AlBahily, K.; Vinu, A. Emerging Trends in Porous Materials for CO<sub>2</sub> Capture and Conversion. *Chem. Soc. Rev.* **2020**, *49* (13), 4360–4404.
- (13) Bahamon, D.; Vega, L. F. Systematic Evaluation of Materials for Post-Combustion CO<sub>2</sub> Capture in a Temperature Swing Adsorption Process. *Chem. Eng. J.* **2016**, *284*, 438–447.
- (14) Shalini, S.; Nandi, S.; Justin, A.; Maity, R.; Vaidhyanathan, R. Potential of Ultramicroporous Metal-Organic Frameworks in CO<sub>2</sub> Clean-Up. *Chem. Commun.* **2018**, *54* (96), 13472–13490.
- (15) Regufe, M. J.; Ferreira, A. F.; Loureiro, J. M.; Rodrigues, A.; Ribeiro, A. M. Electrical Conductive 3D-Printed Monolith Adsorbent for CO<sub>2</sub> Capture. *Microporous Mesoporous Mater.* **2019**, *278*, 403–413.
- (16) Li, J.-R.; Yu, J.; Lu, W.; Sun, L.-B.; Sculley, J.; Balbuena, P. B.; Zhou, H.-C. Porous Materials with Pre-Designed Single-Molecule Traps for CO<sub>2</sub> Selective Adsorption. *Nat. Commun.* **2013**, *4* (1), 1538.
- (17) Hiraide, S.; Sakanaka, Y.; Kajiro, H.; Kawaguchi, S.; Miyahara, M. T.; Tanaka, H. High-Throughput Gas Separation by Flexible Metal-Organic Frameworks with Fast Gating and Thermal Management Capabilities. *Nat. Commun.* **2020**, *11* (1), 3867.
- (18) Yao, Z.-Y.; Guo, J.-H.; Wang, P.; Liu, Y.; Guo, F.; Sun, W.-Y. Controlled Synthesis of Micro/Nanoscale Mg-MOF-74 Materials and Their Adsorption Property. *Mater. Lett.* **2018**, *223*, 174–177.
- (19) Balogun, H.; Bahamon, D.; Almenhali, S.; Vega, L. F.; AlHajaj, A. Are We Missing Something when Evaluating Adsorbents for CO<sub>2</sub> Capture at System Level? *Energy Environ. Sci.* **2021**, *14*, 6360–6380.
- (20) Mason, J. A.; Oktawiec, J.; Taylor, M. K.; Hudson, M. R.; Rodriguez, J.; Bachman, J. E.; Gonzalez, M. I.; Cervellino, A.; Guagliardi, A.; Brown, C. M.; Llewellyn, P. L.; Masciocchi, N.; Long, J. R. Methane Storage in Flexible Metal-Organic Frameworks with Intrinsic Thermal Management. *Nature* **2015**, *527* (7578), 357–361.
- (21) Li, J.-R.; Kuppler, R. J.; Zhou, H.-C. Selective Gas Adsorption and Separation in Metal-Organic Frameworks. *Chem. Soc. Rev.* **2009**, *38* (5), 1477–1504.
- (22) Wang, Q.; Ke, T.; Yang, L.; Zhang, Z.; Cui, X.; Bao, Z.; Ren, Q.; Yang, Q.; Xing, H. Separation of Xe from Kr with Record Selectivity and Productivity in Anion-Pillared Ultramicroporous Materials by Inverse Size-Sieving. *Angew. Chem., Int. Ed.* **2020**, *132* (9), 3451–3456.
- (23) Wang, X.; Krishna, R.; Li, L.; Wang, B.; He, T.; Zhang, Y.-Z.; Li, J.-R.; Li, J. Guest-Dependent Pressure Induced Gate-Opening Effect Enables Effective Separation of Propene and Propane in a Flexible MOF. *Chem. Eng. J.* **2018**, *346*, 489–496.
- (24) Chen, Y.; Qiao, Z.; Lv, D.; Duan, C.; Sun, X.; Wu, H.; Shi, R.; Xia, Q.; Li, Z. Efficient Adsorptive Separation of C<sub>3</sub>H<sub>6</sub> over C<sub>3</sub>H<sub>8</sub> on Flexible and Thermoresponsive CPL-1. *Chem. Eng. J.* **2017**, *328*, 360–367.
- (25) Chang, Z.; Yang, D. H.; Xu, J.; Hu, T. L.; Bu, X. H. Flexible Metal-Organic Frameworks: Recent Advances and Potential Applications. *Adv. Mater.* **2015**, *27* (36), 5432–5441.
- (26) He, T.; Kong, X.-J.; Li, J.-R. Chemically Stable Metal-Organic Frameworks: Rational Construction and Application Expansion. *Acc. Chem. Res.* **2021**, *54* (15), 3083–3094.
- (27) Kong, X.-J.; Li, J.-R. An Overview of Metal-Organic Frameworks for Green Chemical Engineering. *Engineering* **2021**, *7* (8), 1115–1139.
- (28) Chen, Y.; Qiao, Z.; Huang, J.; Wu, H.; Xiao, J.; Xia, Q.; Xi, H.; Hu, J.; Zhou, J.; Li, Z. Unusual Moisture-Enhanced CO<sub>2</sub> Capture Within Microporous PCN-250 Frameworks. *ACS Appl. Mater. Interfaces* **2018**, *10* (44), 38638–38647.
- (29) Sabouni, R.; Kazemian, H.; Rohani, S. Carbon Dioxide Capturing Technologies: a Review Focusing on Metal Organic Framework Materials (MOFs). *Environ. Sci. Pollut. Res.* **2014**, *21* (8), 5427–5449.
- (30) Li, B.; Chen, B. A Flexible Metal-Organic Framework with Double Interpenetration for Highly Selective CO<sub>2</sub> Capture at Room Temperature. *Sci. China Chem.* **2016**, *59* (8), 965–969.
- (31) Yang, J.; Yu, Q.; Zhao, Q.; Liang, J.; Dong, J.; Li, J. Adsorption CO<sub>2</sub>, CH<sub>4</sub> and N<sub>2</sub> on Two Different Spacing Flexible Layer MOFs. *Microporous Mesoporous Mater.* **2012**, *161*, 154–159.
- (32) Nijem, N.; Thissen, P.; Yao, Y.; Longo, R. C.; Roodenko, K.; Wu, H.; Zhao, Y.; Cho, K.; Li, J.; Langreth, D. C.; Chabal, Y. J. Understanding the Preferential Adsorption of CO<sub>2</sub> over N<sub>2</sub> in a Flexible Metal-Organic Framework. *J. Am. Chem. Soc.* **2011**, *133* (32), 12849–12857.
- (33) Wu, H.; Reali, R. S.; Smith, D. A.; Trachtenberg, M. C.; Li, J. Highly Selective CO<sub>2</sub> Capture by a Flexible Microporous Metal-Organic Framework (MMOF) Material. *Chem.—Eur. J.* **2010**, *16* (47), 13951–13954.
- (34) Singh, H. D.; Nandi, S.; Chakraborty, D.; Singh, K.; Vinod, C. P.; Vaidhyanathan, R. Coordination Flexibility Aided CO<sub>2</sub>-specific Gating in an Iron Isonicotinate MOF. *Chem.—Asian J.* **2022**, *17* (4), No. e202101305.
- (35) Sotomayor, F. J.; Lastoskie, C. M. Carbon Dioxide Capacity Retention on Elastic Layered Metal Organic Frameworks Subjected to Hydrothermal Cycling. *Microporous Mesoporous Mater.* **2020**, *292*, 109371.
- (36) Hiraide, S.; Tanaka, H.; Ishikawa, N.; Miyahara, M. T. Intrinsic Thermal Management Capabilities of Flexible Metal-Organic Frameworks for Carbon Dioxide Separation and Capture. *ACS Appl. Mater. Interfaces* **2017**, *9* (46), 41066–41077.
- (37) Arami-Niya, A.; Birkett, G.; Zhu, Z.; Rufford, T. E. Gate Opening Effect of Zeolitic Imidazolate Framework ZIF-7 for Adsorption of CH<sub>4</sub> and CO<sub>2</sub> from N<sub>2</sub>. *J. Mater. Chem. A* **2017**, *5* (40), 21389–21399.
- (38) Wu, X.; Shahrak, M. N.; Yuan, B.; Deng, S. Synthesis and Characterization of Zeolitic Imidazolate Framework ZIF-7 for CO<sub>2</sub>



and CH<sub>4</sub> Separation. *Microporous Mesoporous Mater.* **2014**, *190*, 189–196.

(39) Arunan, E.; Desiraju, G. R.; Klein, R. A.; Sadlej, J.; Scheiner, S.; Alkorta, I.; Clary, D. C.; Crabtree, R. H.; Dannenberg, J. J.; Hobza, P. Definition of the Hydrogen Bond (IUPAC Recommendations 2011). *Pure Appl. Chem.* **2011**, *83* (8), 1637–1641.

(40) Hubbard, R. E.; Haider, M. K. Hydrogen Bonds in Proteins: Role and Strength. *eLS*; Wiley, 2010; DOI: 10.1002/9780470015902.a0003011.pub2.

(41) Hyun, S.-M.; Lee, J. H.; Jung, G. Y.; Kim, Y. K.; Kim, T. K.; Jeoung, S.; Kwak, S. K.; Moon, D.; Moon, H. R. Exploration of Gate-Opening and Breathing Phenomena in a Tailored Flexible Metal-Organic Framework. *Inorg. Chem.* **2016**, *55* (4), 1920–1925.

(42) Zhang, X.-W.; Zhou, D.-D.; Zhang, J.-P. Tuning the Gating Energy Barrier of Metal-Organic Framework for Molecular Sieving. *Chem* **2021**, *7* (4), 1006–1019.

(43) Liu, B.; Zhao, R.; Yang, G.; Hou, L.; Wang, Y.-Y.; Shi, Q.-Z. Two isostructural amine-functionalized 3D self-penetrating microporous MOFs exhibiting high sorption selectivity for CO<sub>2</sub>. *CrystEngComm* **2013**, *15* (11), 2057–2060.

(44) *Materials Studio*, version 7.0; Biovia Software Inc.: San Diego, CA 92121, USA.

(45) Furukawa, H.; Gandara, F.; Zhang, Y.-B.; Jiang, J.; Queen, W. L.; Hudson, M. R.; Yaghi, O. M. Water Adsorption in Porous Metal-Organic Frameworks and Related Materials. *J. Am. Chem. Soc.* **2014**, *136* (11), 4369–4381.

(46) Yang, R. T. *Adsorbents: Fundamentals and Applications*; John Wiley & Sons, 2003.

(47) Valenzuela, D. P.; Myers, A. L. In *Adsorption Equilibrium Data Handbook*; Prentice Hall: Englewood Cliffs, NJ, 1989.

(48) Xiong, S.; Liu, Q.; Wang, Q.; Li, W.; Tang, Y.; Wang, X.; Hu, S.; Chen, B. A Flexible Zinc Tetrazolate Framework Exhibiting Breathing Behaviour on Xenon Adsorption and Selective Adsorption of Xenon over Other Noble Gases. *J. Mater. Chem. A* **2015**, *3* (20), 10747–10752.

(49) McGuirk, C. M.; Runcevski, T.; Oktawiec, J.; Turkiewicz, A.; Taylor, M. K.; Long, J. R. Influence of Metal Substitution on the Pressure-Induced Phase Change in Flexible Zeolitic Imidazolate Frameworks. *J. Am. Chem. Soc.* **2018**, *140* (46), 15924–15933.